Meteorol Atmos Phys (2011) 113:11–25
DOI 10.1007/s00703-011-0147-7

ORIGINAL PAPER

An exceptionally heavy snowfall in Northeast china: large-scale circulation anomalies and hindcast of the NCAR WRF model

Huijun Wang · Entao Yu · Song Yang

Received: 29 March 2011 / Accepted: 25 May 2011 / Published online: 8 June 2011

Abstract In Northeast China (NEC), snowfalls usually occur during winter and early spring, from mid-October to late March, and strong snowfalls rarely occur in middle spring. During 12–13 April 2010, an exceptionally strong snowfall occurred in NEC, with 26.8 mm of accumulated water-equivalent snow over Harbin, the capital of the most eastern province in NEC. In this study, the major features of the snowfall and associated large-scale circulation and the predictability of the snowfall are analyzed using both observations and models. The Siberia High intensified and shifted southeastward from 10 days before the snowfall, resulting in intensifying the low-pressure system over NEC and strengthening the East Asian Trough during 12–13 April. Therefore, large convergence of water vapor and strong rising motion appeared over eastern NEC, resulting in heavy snowfall. Hindcast experiments were carried out using the NCAR Weather Research and Forecasting (WRF) model in a two-way nesting approach, forced by NCEP Global Forecast System data sets. Many observed features including the large-scale and regional circulation anomalies and snowfall amount can be reproduced reasonably well, suggesting the feasibility of the WRF model in forecasting extreme weather events over NEC. A quantitative analysis also shows that the nested NEC domain simulation is even better than mother domain simulation in simulating the snowfall amount and spatial distribution, and that both simulations are more skillful than the NCEP Global Forecast System output. The forecast result from the nested forecast system is very promising for an operational purpose.

Responsible editor: S. Trini Castelli.

H. Wang (✉) · E. Yu
Nansen-Zhu International Research Center,
Institute of Atmospheric Physics,
Chinese Academy of Sciences, Beijing, China
e-mail: wanghj@mail.iap.ac.cn

H. Wang · E. Yu
Climate Change Research Center, Institute of Atmospheric Physics, Chinese Academy of Sciences, Beijing, China

E. Yu
Graduate University of Chinese Academy of Sciences, Beijing, China

S. Yang
NOAA Climate Prediction Center, Camp Springs, MD, USA

1 Introduction

During winter and early spring, snowfalls occur frequently in Northeast China (NEC). Strong snowfalls often cause damages to pasturage and other properties and bring hazardous conditions to transportation and other human activities. Therefore, numerous studies have been conducted to understand the formation, mechanisms and predictability of snowstorms (Wang and Ding 1995; Zielinski 2002; Zhang et al. 2002; Kocin and Uccellini 2004; Changnon et al. 2006; Sun et al. 2010). Anomalous atmospheric circulation both in the troposphere and stratosphere is associated with the snowstorm and cold surge in East Asia (Sun et al. 2009; Jeong et al. 2006). However, for mid-spring snowstorms, which are less frequent and should have different physical mechanisms from those of winter and early spring snowstorms, there have been fewer studies. Sun et al. (2009) suggested that the troposphere atmospheric circulation anomalies over mid-high latitudes play a crucial role in a strong snowstorm over NEC during 3–5 March 2007. They found persistent anomalies in the Arctic Oscillation (Thompson and Wallace 1998; Gong et al. 2001), the North

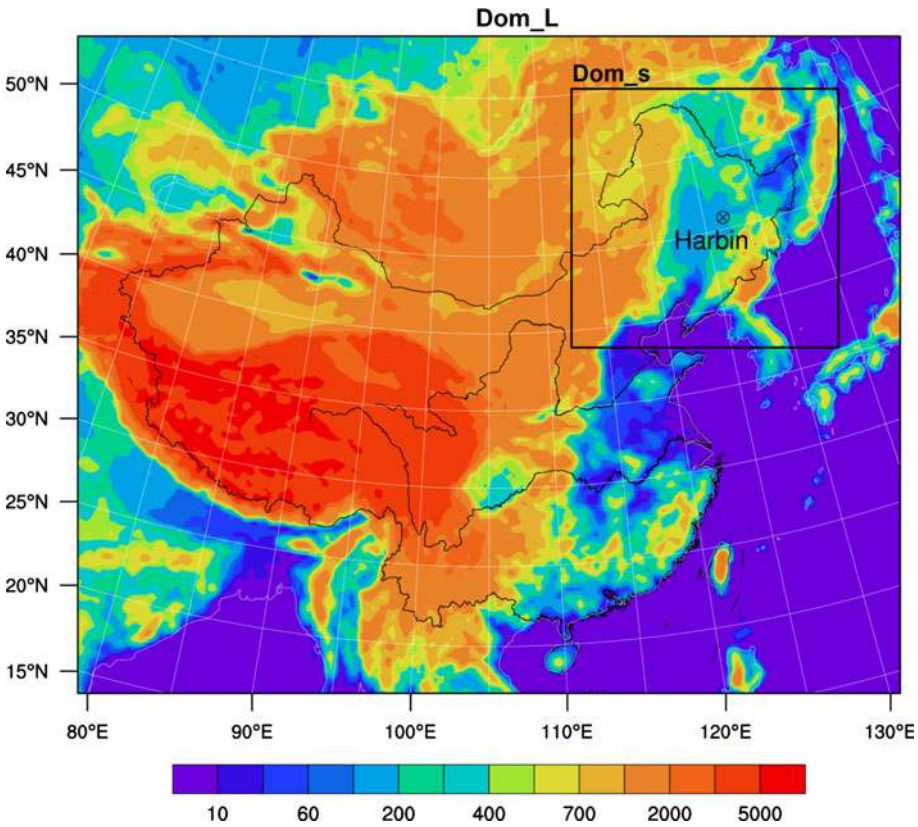

Fig. 1 Domains for two-way nesting hindcast experiments and the topography (*color shading*)

Pacific Oscillation (Wallace and Gutzler 1981), and the Eurasian teleconnection pattern (Gambo et al. 1987) before the snowstorm. Besides the mid-high latitude effect, Qin and Jin (2008) indicated a significant role of the northeastward moving vortex that originated from Southwest China in NEC snowstorms. The recent study by Liu et al. (2010) showed that both frequency and intensity of the snowstorms in Heilongjiang Province have increased in the past 50 years.

Regional climate models have also been used to study the precipitation processes in China (Liu et al. 1994, 1996, 2008; Xu et al. 2007; Qin and Jin 2008). In particular, Qin and Jin (2008) used the PSU/NCAR Mesoscale Model (MM5) to study the above-mentioned heavy snowstorm during 3–5 March 2007. However, no attempt has been made to investigate the predictability of the strong snowstorms over NEC in mid-spring using numerical weather forecast models.

An exceptionally heavy snowstorm occurred in NEC during 12–13 April 2010. In 29 counties of the Heilongjiang Province, the water-equivalent snow amount exceeded 10 mm, with more than 26.8 mm in Harbin, the capital city of the Heilongjiang Province. The daily mean temperature dropped abruptly by more than 10°C in much of the province due to the effect of the snowstorm. In Harbin, the amount of water-equivalent snow broke the record of 50 years. Another April heavy snowfall was recorded on 29 April 1983, but is was accompanied by much less precipitation amount.

We carry out this study for two main purposes. First, we attempt to understand the large-scale atmospheric circulation anomalies, both local and remote, which were associated with the exceptionally strong snowstorm over NEC during 12–13 April 2010. We investigate the feasibility of regional weather models, forced by boundary data of real-time analyses or by global numerical models, in forecasting such strong snowstorm over NEC.

In the next section, we describe the model and experiment design. In Sect. 3 , we discuss the evolution of large-scale circulation patterns associated with the snowstorm. Results from retrospective forecast experiments, including quantitative verification on water-equivalent snow process, are discussed in Sect. 4. A summary is provided in Sect. 5.

2 Model and design of numerical experiments

The Weather Research and Forecasting (WRF) model was developed in a collaborative effort by the National Center for Atmospheric Research (NCAR), the National Centers for Environmental Prediction (NCEP), the Forecast Systems Laboratory, the Air Force Weather Agency, Oklahoma University and other institutions (Purser et al. 2001). It is a non-hydrostatic mesoscale weather modeling system, with flexible resolutions and parameterization schemes.

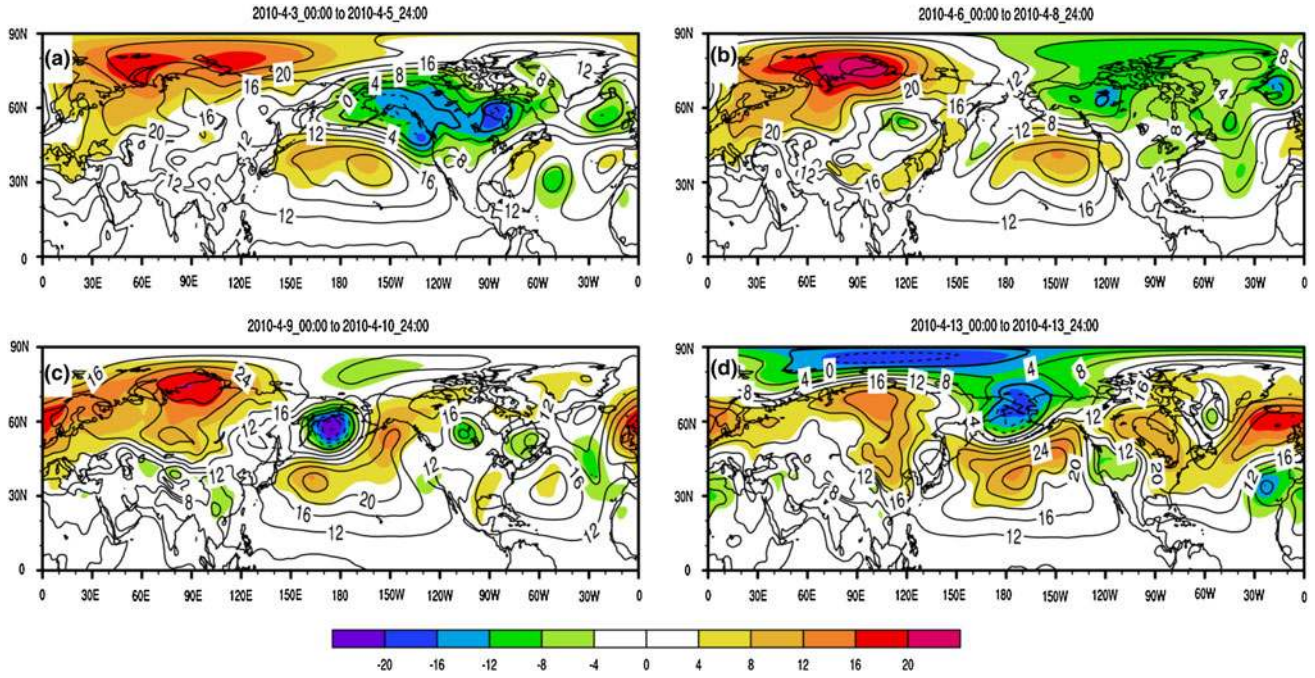

Fig. 2 Evolution of observed geopotential height (in degpm, *contour*) and its anomaly (in degpm, *color shading*) at 1,000 hPa during 3–13 April 2010. The anomalies refer to the departures from the averages for 1989–2009

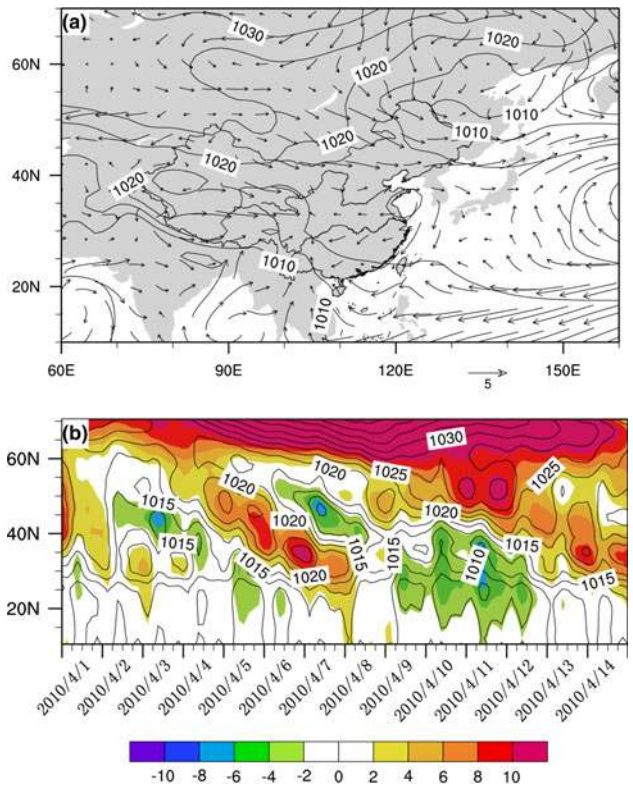

Fig. 3 a Distribution of SLP (*contour*, in hPa) and surface wind (in m/s) averaged over the period 1–14 April 2010. b Latitude–time evolution of the sea-level pressure (*contour*, in hPa) averaged over 70–130°E and its anomaly (*color shading*, in hPa)

The version of WRF model used in this study has horizontal resolutions of 45 and 15 km, and has 28 sigma levels with the model top at 50 hPa. It is used for two-way nested domains: DOM_L and DOM_S (see Fig. 1). The model mother domain (DOM_L) covers the entire mainland China with 140 grids in the east–west direction and 120 grids in the north–south direction. The nested domain (DOM_S) focuses mainly on NEC with 100 grids in both east–west and north–south directions. A two-way nesting approach was applied in this research, meaning that all quantities were interactive between DOM_L and DOM_S.

The WRF Single-Moment 6-Class Scheme is used for the micro-physical process, and other options are configured as the Kain-Fritsch Scheme for cumulus convective parameterization (Kain and Fritsch 1993), Rapid Radiative Transfer Model (Mlawer et al. 1997) for longwave radiation, Dudhia scheme (Dudhia 1989) for shortwave radiation, Yonsei University planetary boundary layer parameterization (Hong et al. 2006) and the Noah (NCEP, Oregon State University, Air Force and Hydrologic Research Laboratory) land surface model with four layers of soil.

The global forecast system (GFS) 6 hourly data sets in $1 \times 1°$ resolution are used, respectively, as the initial and boundary conditions for model experiments. Validation for the forecast is based on meteorological station data and the ERA-Interim data set in $1.5 \times 1.5°$ resolution. The ERA-Interim represents a major undertaking by ECMWF (the

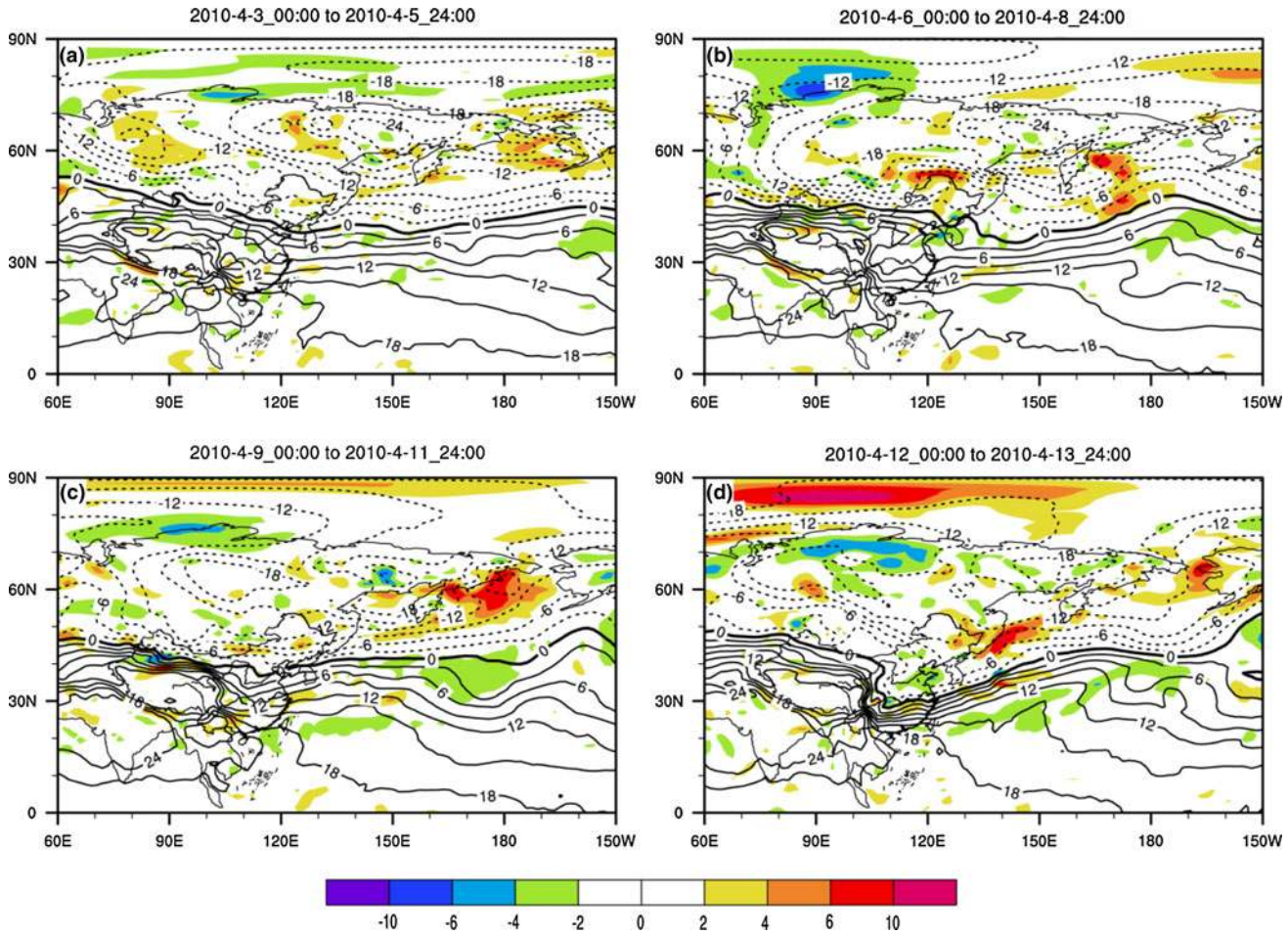

Fig. 4 Evolution of observed temperature (in °C, *contours*) and vorticity (in 10^{-5} s^{-1} *color shading*) at 850 hPa for 3–13 April 2010

European Centre for Medium-Range Weather Forecasts) to produce a reanalysis with improved atmospheric model and assimilation system, which replace those used in ERA-40, particularly for the data-rich 1990s and 2000s. It is to be continued as an ECMWF Climate Data Assimilation System until superseded by a new extended reanalysis (Simmons et al. 2007). The experiments are initiated from 00:00 GMT on the 11th of April 2010. To summarize, a pair of numerical experiments was performed for DOM_L and DOM_S starting from 00:00 GMT of 11 April and forced by the GFS data.

3 Evolution of large-scale circulation

Before the heavy snow process on 12–13 April 2010 (referred to as HS1004 for convenience), a strong high-pressure system appeared over the high latitudes of Eurasia 10 days before the snowstorm (Fig. 2), indicating that the Siberia High was in an intensified phase. Then the Siberia High kept intensifying and expanding southeastward until the snowstorm occurred. As a result, the northwest winds over northeastern Asia also enhanced and shifted southeastward. It can also be seen from Fig. 2, which shows the anomalies relative to the 1989–2009 averages, that the global zonal structure of low-level pressure resembles a wave number-one pattern in high latitudes, with positive anomalies over Eurasia and negative anomalies over North America. The North Pacific Oscillation was in a strong negative phase, thus the negative and positive sea-level pressure anomalies were located in the north and south like a dipole pattern. Figure 3a clearly indicates that strong northwesterly wind prevailed at 1,000 hPa over northeastern Asia, forming strong cold air advection to NEC. Meanwhile, the strong cold air advection favored the development of anomalous low pressure in NEC (Fig. 2). In large areas of Eurasia, high-pressure anomalies over a large part of Europe were accompanied by northwesterly wind and resulted in southeastward shift of low-pressure system.

Figure 3b well describes the southward expansion of the high-pressure system (anomalies shaded by red color)

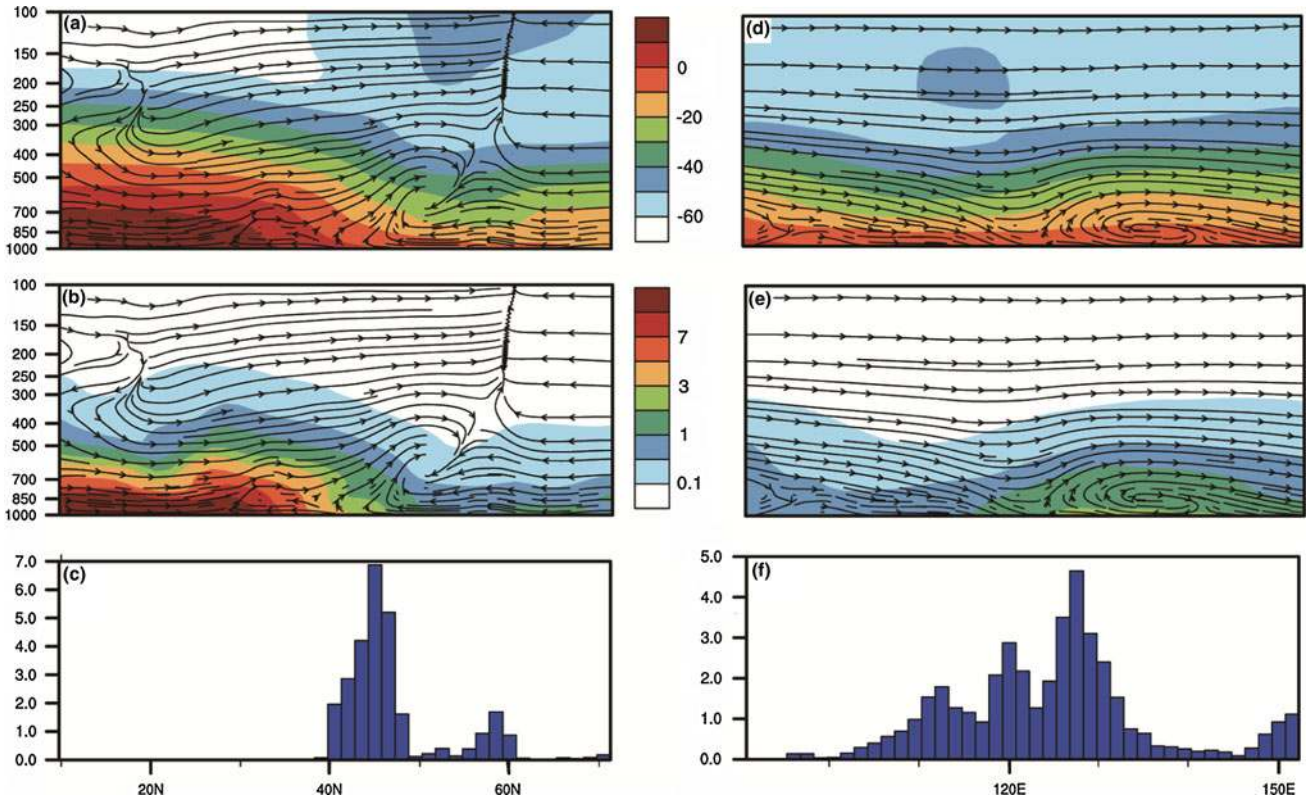

Fig. 5 Vertical thermal-dynamic structure for 12 April. **a** Averaged vertical circulations (*streamlines*) and temperature (*color shading*) in a south–north vertical cross section averaged for 120–130°E. **b** Same as **a**, but for specific humidity (in g/kg). **c** Mean water-equivalent snow (in mm) averaged for 120–130°E. **d** and **e** are corresponding to **a** and **b**, but for the west–east vertical cross section averaged for 40–55°N. **e** Mean water-equivalent snow (in mm) averaged for 40–55°N

averaged to 70°E–130°E from high latitudes to low latitudes from 1 April to 14 April (in 336 h). In the meantime, the low-pressure system (anomalies shaded by green color) was pushed further south. We note that the negative anomalies were at the magnitude of −2 to −6 hPa, and the positive anomalies were much larger (at 8–10 hPa). This continuous southward expansion and propagation naturally resulted in the cold air development and advection from high latitudes to middle latitudes. Due to the strengthening and southeastward expansion of the Siberia High and the advection of negative pressure and temperature anomalies, the low-pressure system over NEC further deepened on 12–13 April.

To illustrate the associated thermal-dynamic environment, Fig. 4 shows the evolution processes of air temperature and vorticity at 850 hPa. The center of low temperature was located over Siberia and North Pacific, and because of the continuous cold air advection from Siberia to NEC, the temperature over NEC remained below freezing and dropped gradually with time before 12 April. Along with the abrupt deepening of the low-pressure system and the advection of cold air over NEC, the temperature dropped more significantly on 12–13 April, with temperature lower than −9°C at 850 hPa over much of NEC and an even colder condition over Heilongjiang Province (in eastern NEC). In the meantime, the positive vorticity over NEC also intensified gradually before 12 April and strengthened suddenly during 12–13 April, associated with the development of low-pressure system. The intensified low-pressure system and strong positive vorticity reinforced the atmospheric convection and rising motion over NEC. Meanwhile, the northwesterly flow over NEC persistently transported water vapor to the eastern part of NEC before 12 April. During 12–13 April, much stronger convergence of water vapor occurred over eastern NEC, which resulted from the combined effects of the northwesterly flow from Eurasia and the easterly flow at 1,000 hPa from the North Pacific. The easterly flow from the North Pacific is mainly the result of the low-level low-pressure system over NEC and the high pressure over the northwestern Pacific. Consequently, the HS1004 event occurred on 12–13 April, with the peak on 13 April. Similar patterns can also be found in the velocity and specific humidity at 850 hPa.

At 500 hPa, the mid-high latitude region of Eurasia was occupied by a blocking high system and the northwestern Pacific was covered by positive anomalies as well, whereas eastern Siberia was covered by a low-pressure circulation.

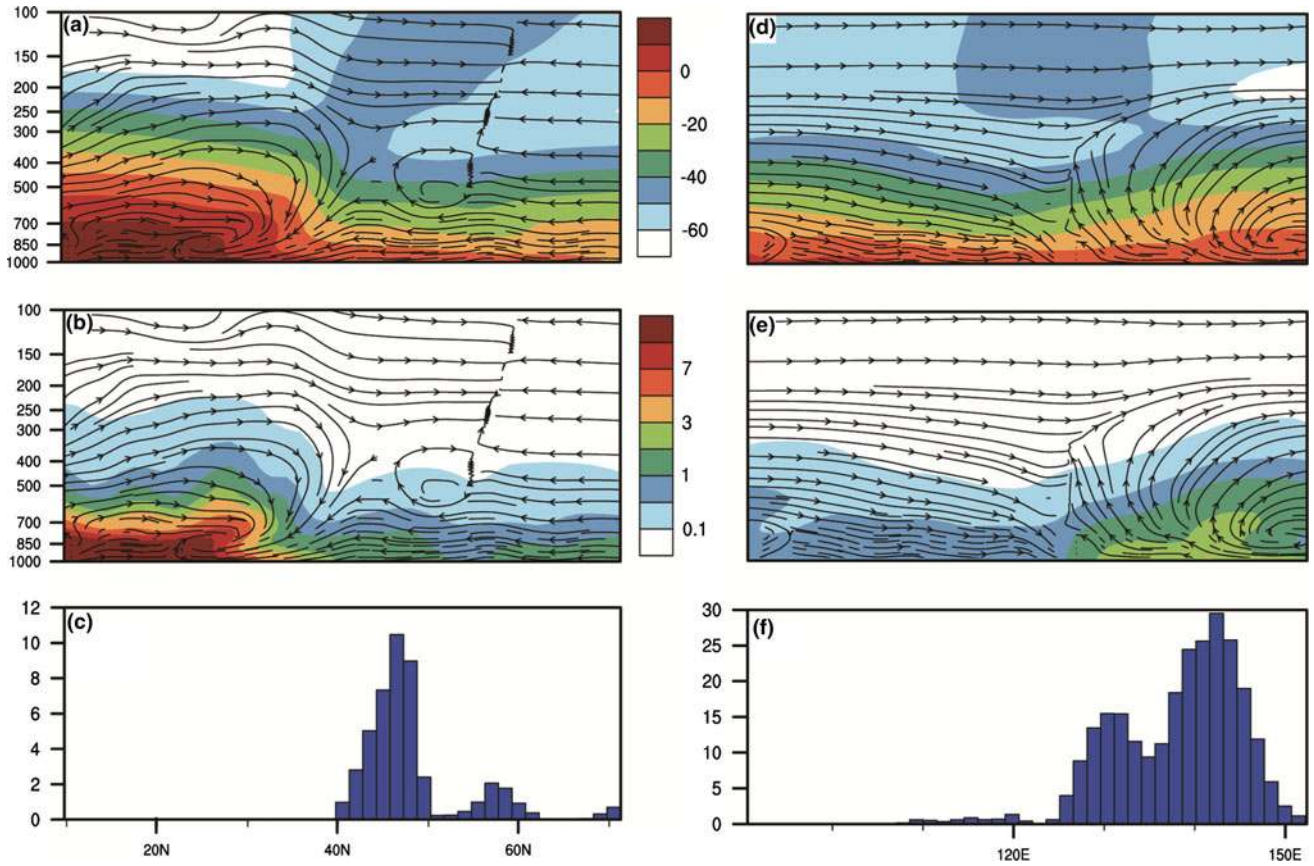

Fig. 6 As in Fig. 5, but for 13 April 2010

Thus, the East Asian Trough, a planetary trough that exerts strong impact on the weather and climate in East Asia (Wang and Jiang 2004), deepened along 120°E during the pre-HS1004 period. Deepening of the trough, associated with strong cold air advection from the high latitudes, indicates intensifications of vertical convection and low-pressure system at the lower atmosphere. For the case of HS1004, the cold air advection to NEC was particularly strong because the center of the cold air was located behind (i.e. to the west of) the trough. In addition, the southern annular mode was in the positive phase during 12–13 April. This can be demonstrated by the sea-level pressure pattern, indicating the Antarctic circumpolar low was in the deepened phase after 9 April. The positive anomaly of the southern annular mode was documented to be associated with intensification and westward expansion of the western Pacific subtropical high (Xue et al. 2003). This is favorable to the strengthening of the East Asian Trough and the low-level low-pressure system over NEC.

Now, we depict the vertical picture associated with HS1004. Figure 5 indicates the latitude–height cross section for zonal mean of 120°E–130°E (by Fig. 5a–c) and longitude–height cross section for meridional mean of 40–55°N (by Fig. 5d–f) averaged 00:00–18:00 GMT of 12 April. For this period, snowfall occurred mainly in the central and western NEC (to the west of 130°E). The cross section for air temperature and stream lines well indicates the cold front genesis (Fig. 5a). In the low-level atmosphere, both the meridional and zonal winds contributed to convergence to NEC and the cyclonic circulation. Meanwhile, the water vapor converges to NEC jointly from the westward, eastward and northward. However, the snowfall amount is much smaller compared to that of the following day. This is because the convergence was still not very large enough, as the easterly winds were weak then.

Since the snowfall almost stopped at 12:00 on 13 April, Fig. 6 shows the picture for 00:00–12:00 on 13 April, corresponding to Fig. 5. We can find that the major difference is the eastward moving and intensification of the snowstorm system. The snowfall is mainly located to the east of 130°E and the snow amount is much larger than the previous day. One reason for the intensification is the strengthening of low-level easterly wind and associated eastward water vapor transport to eastern NEC. Another reason is the stronger low-level convergence of the stream flow and associated vertical motion. Intensification of vertical motion is partly because of strengthening of the easterly wind and the associated convergence in the low

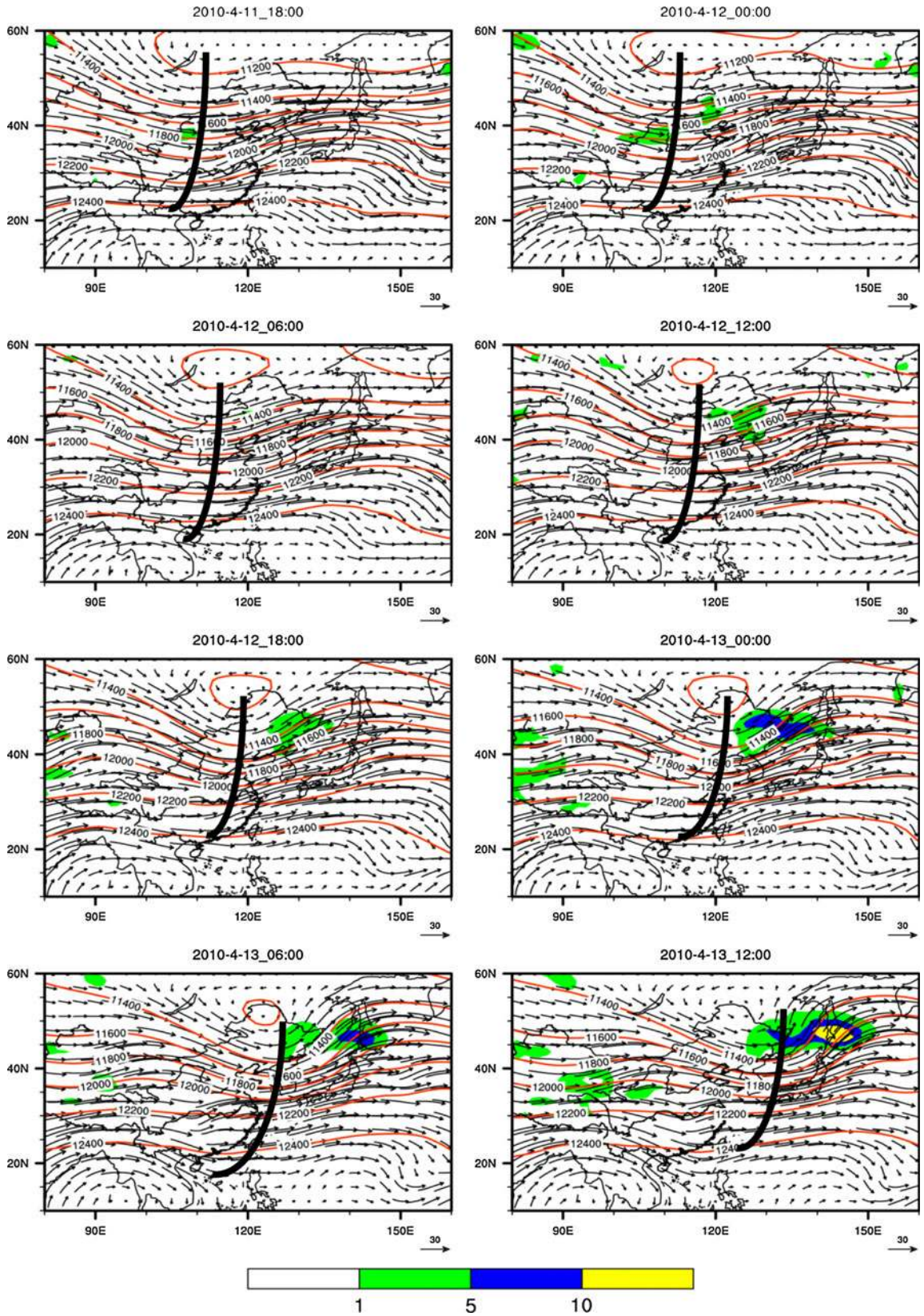

Fig. 7 The evolution process for geopotential height (in degpm, by *contour*), velocity (in m/s, by *vector*) and water-equivalent snow (in mm, by shading) at 200 hPa during 18:00 on April 11 to 12:00 on April 13. The *thick black lines* indicate the East Asian Trough

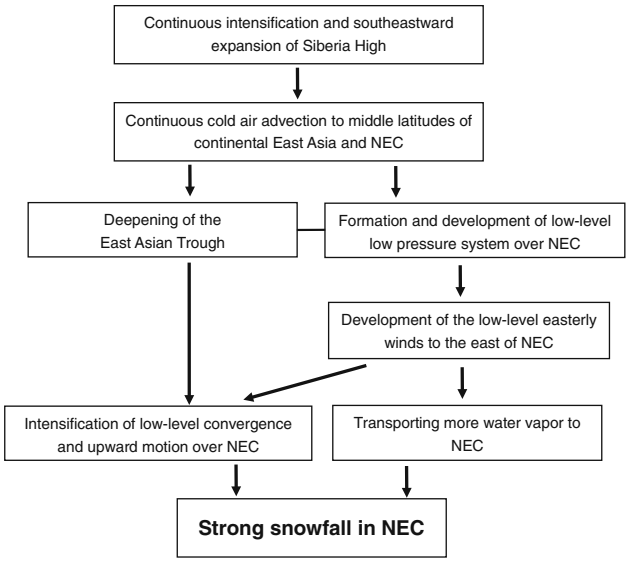

Fig. 8 The schematic overall evolution process of the large-scale atmospheric circulation associated with the snowstorm HS1004

levels and partly because of deepening of the East Asian Trough. Deepening of the East Asian Trough, the continuous cold air advection to NEC and the intensification of the western Pacific subtropical high favor the strengthening of the low-level convergence and high-level divergence.

The East Asian Trough enhancement can be demonstrated more clearly by the velocity and geopotential height at 200 hPa (Fig. 7), where the westerly jet kept in the intensified phase during 11–13 April and the East Asian Trough kept moving from northwest to southeast. It kept moving further and arrived at the coastal region of Eastern China and Eastern China Sea. In northern and eastern NEC, cyclonic and anticyclonic circulation developed. Thus, the picture for 12–13 April over the eastern NEC, the region with heavy snowfall, includes the intensified low-level convergence, high-level divergence and vertical motion in the middle and low troposphere.

When discussing about water vapor transport to NEC, we have not yet mentioned the contribution from the southerly winds. As a matter of fact, there was a southerly component of water vapor transport to NEC, but only for 12 April and not for 13 April (see Figs. 5b, 6b). This southerly component is quite important for the snowfall of 12 April, because the water content was much higher in the low latitude than in the high latitude over East Asia.

Therefore, the schematic illustration of the snowstorm overall process in eastern NEC may be expressed in Fig. 8. The positive geopotential height anomalies in high-latitude Eurasia expanded and moved continuously southeastward before the HS1004, along with persistently strong cold air advection at the low and middle troposphere and the intensification and southeastward shift of negative anomalies over the middle-latitude Eurasia. As a result, the low-level pressure and the East Asian Trough further developed on 12–13 April. In the meantime, low-level easterly winds from the Pacific Ocean enhanced the low-level convergence, high-level divergence and vertical motion and transported more water vapor to NEC. Thus, heavy snowfall occurred in eastern NEC during 12–13 April.

The above analysis indicates that the precursory features of HS1004 could be traced back to about 10 days before the snowstorm and they were the anomalous atmospheric circulation systems at both lower and middle troposphere that intensified and shifted southeastward, along with a gradually intensified cold surge, resulting in the cold front and cyclonic circulation over eastern NEC. The combined effects of the exceptionally strong Siberia High, cold surge, cutoff low-pressure system, and East Asian Trough caused HS1004, an exceptionally strong mid-spring snowstorm (strongest in the past 50 years) over eastern NEC.

4 Retrospective forecasts by DOM_L and DOM_S

In this section, we investigate to what extent the WRF-based nesting technique can simulate the heavy snow process HS1004. The extent of the snowfall and the associated atmospheric circulation patterns, simulated by the model, will be analyzed.

We first perform a quantitative comparison between the ERA-Interim and the DOM_L simulation. With respect to the geopotential height and air temperature at 500 hPa for the reanalysis and the simulation, the DOM_L simulation well captures the intensification and the eastward shift of the East Asian Trough from 00:00 on 12 April to 24:00 on 13 April. The model quantitatively well reproduces the geopotential height in the whole domain and in NEC in particular. Both the pattern and the magnitude of air temperature are also well simulated. The center of low temperature tilt behind the center of low geopotential height, and thus the 'temperature trough', is located westward with respect to the East Asia Trough, resulting in strong cold air advection to NEC. This feature is crucial for the cold surge and the developments of front and cyclone in Northeast China. In short, the model captures the large-scale circulation patterns at the mid-troposphere associated with the formation of HS1004.

Moreover, the distribution, magnitude and eastward shift of 850-hPa stream velocity and relative humidity from 00:00 on 12 April to 12:00 on 13 April are well simulated (Fig. 9). The cyclonic circulation in NEC is well captured. One important feature for HS1004 is that the water vapor did not mainly come from South China, as in the case of many snowfalls in NEC. The water vapor for HS1004 was

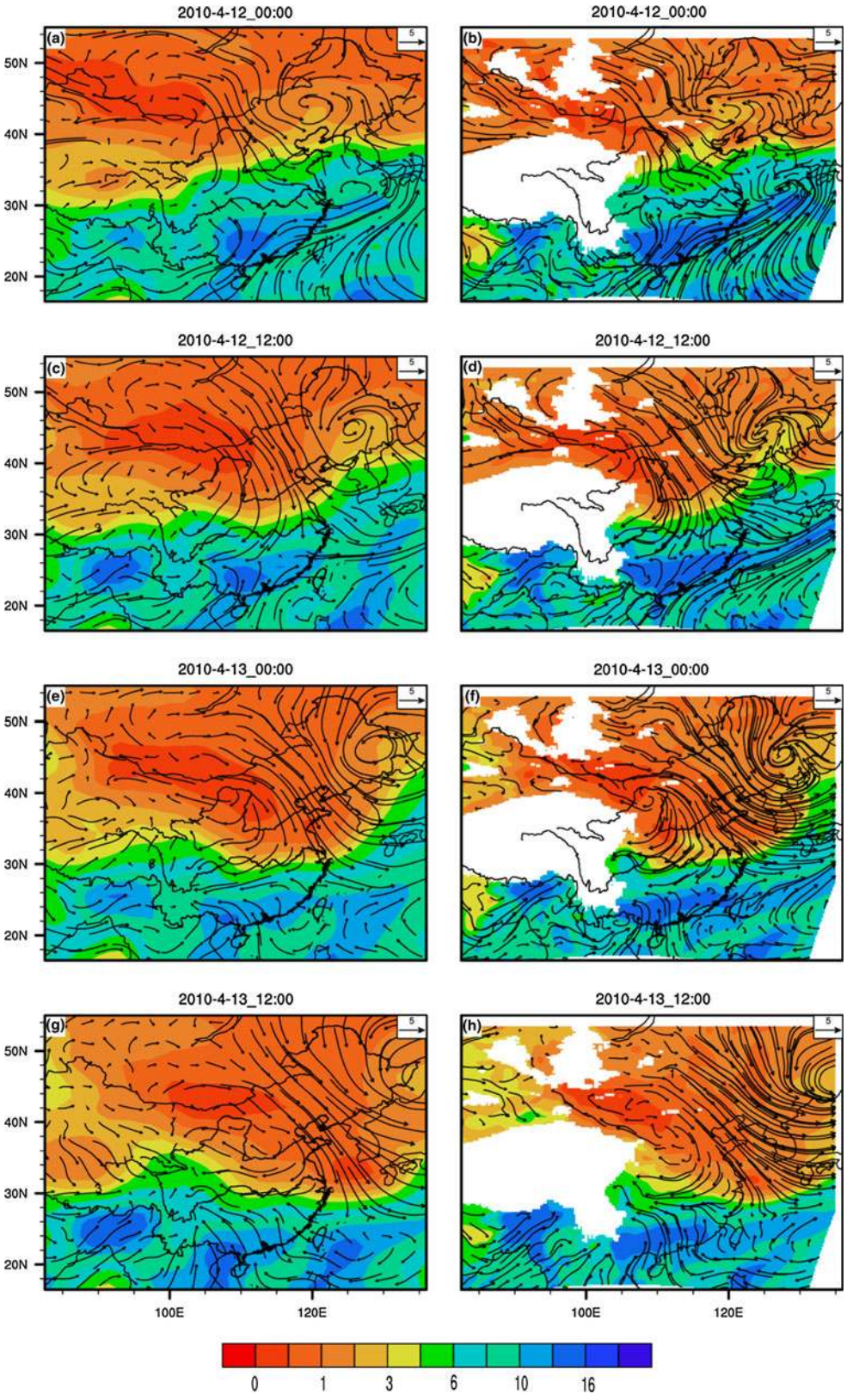

Fig. 9 Observed (*left panels*) and DOM_L simulated (*right panels*) velocity (in m/s, *arrows*) and specific humidity (in g/kg, *color shading*) at 850 hPa for 00:00 and 12:00 of 12 April, and 00:00 and 12:00 of 13 April 2010

transported mainly from the western North Pacific and Northeast Asia. In the temperature evolution during 3–13 April, the lowest temperature at 850 hPa is seen at 00:00 on 13 April (Fig. 10), with values lower than −13°C over much of NEC. The DOM_L simulation well captures these features of time evolution and spatial patterns of air

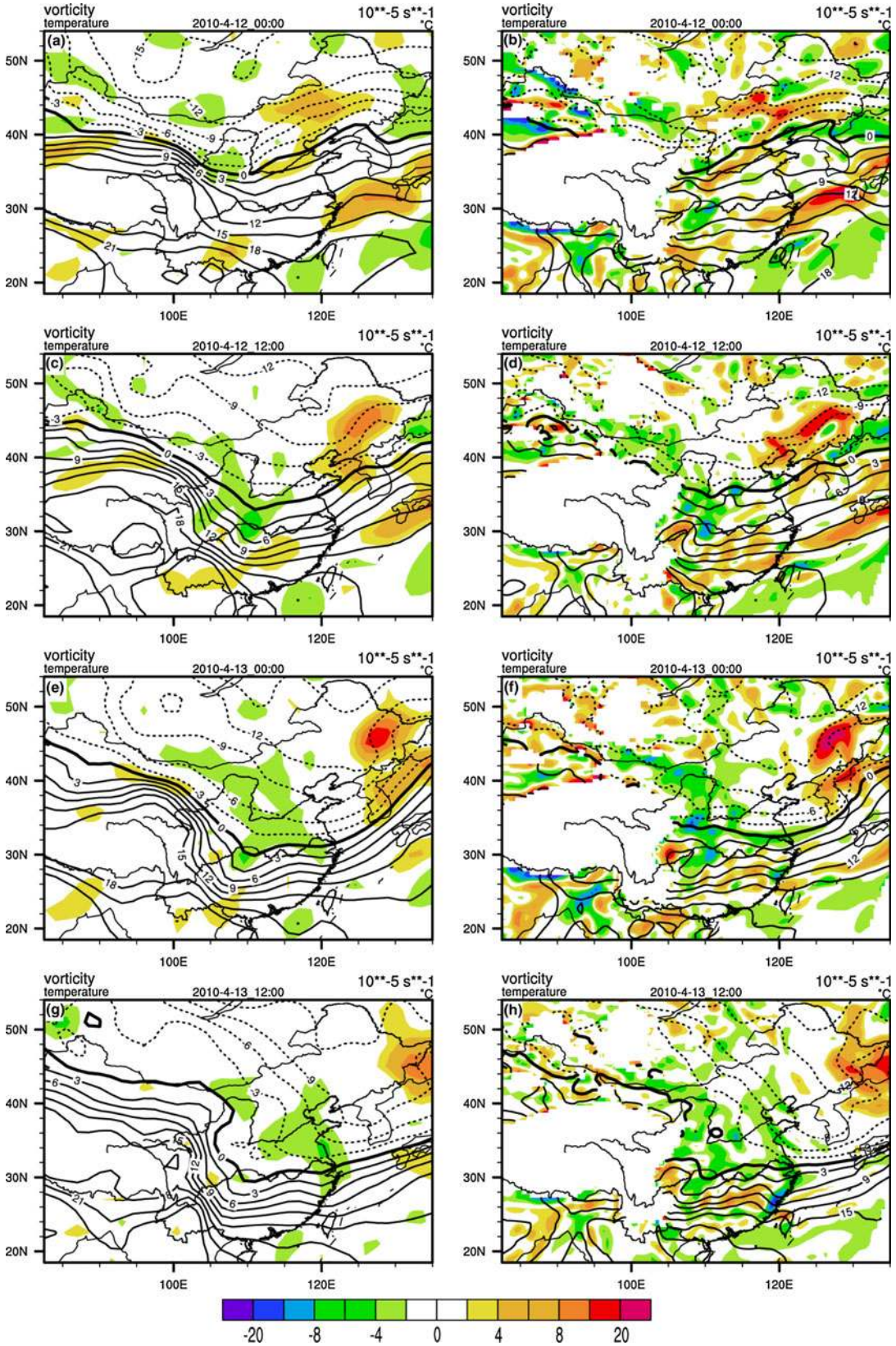

Fig. 10 Observed (*left*) and DOM_L simulated (*right*) temperature (in °C, *contours*) and vorticity (in 10^{-5} s^{-1}, *color shading*) at 850 hPa for 00:00 and 12:00 of 12 April, 00:00 and 12:00 of 13 April 2010

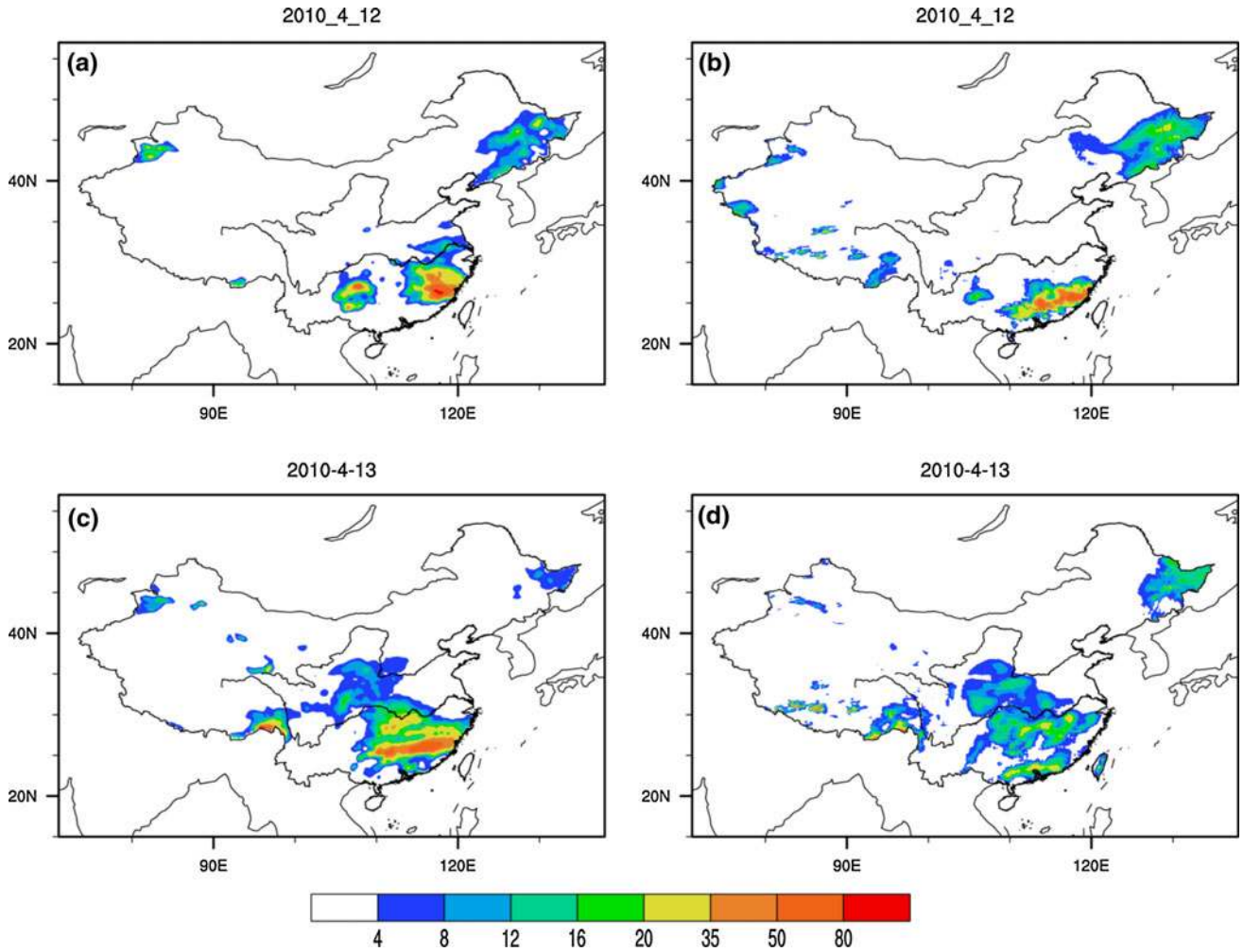

Fig. 11 Observed (*left*) and DOM_L simulated (*right*) 24-h accumulated precipitation (in mm) for 12 (*above*) and 13 (*below*) April 2010

temperature from 00:00 on 12 April to 12:00 on 13 April. However, on 12:00 GMT 13 April, the model simulates lower temperature by about 2°C in eastern NEC as compared to the observation, although the simulation of temperature at 00:00 GMT 13 April is relatively better. Vorticity simulation is generally as realistic as the temperature simulation, in terms of the spatial pattern, temporal evolution and magnitude, despite that the model somewhat tends to over-reproduce the vorticity from 00:00 to 12:00 on 13 April.

In addition, the model systematically overestimates the stream flow over NEC. As a result, the low-level convergence is exaggerated to some extent, as demonstrated by the 700-hPa vertical velocity (figure not shown). An overestimation of rising motion by the model can be clearly seen in the Heilongjiang Province. The sinking motion to the west of NEC is stronger in the simulation than in observations as well. It seems that the model produces larger fluctuations of atmospheric vertical motion than observed over NEC.

We then depict the observed and DOM_L simulated distributions of 24-h total precipitation for 12 and 13 April. Figure 11 shows that the two major precipitation regions in NEC and South China are qualitatively well reproduced. However, in South China, the simulated precipitation for 12 April is largely different with the observation in spatial location and the simulated precipitation for 13 April is smaller than the observation. The big error in South China is mainly associated with the fact that our nesting approach is applied over the NEC region. The snowfall amount in eastern NEC is very well captured for 12 April, but the area of simulated precipitation for 13 April in the Heilongjiang Province extends more westward compared to observations. Since two-way nesting strategy was applied in NEC, the DOM_L provides better simulation on the precipitation over NEC than South China. Therefore, it well demonstrates that dynamical downscaling with WRF can obtain better forecasts for regional precipitation.

The location and amount of 48-h snowfall in eastern NEC are both well simulated by DOM_L. In addition, the

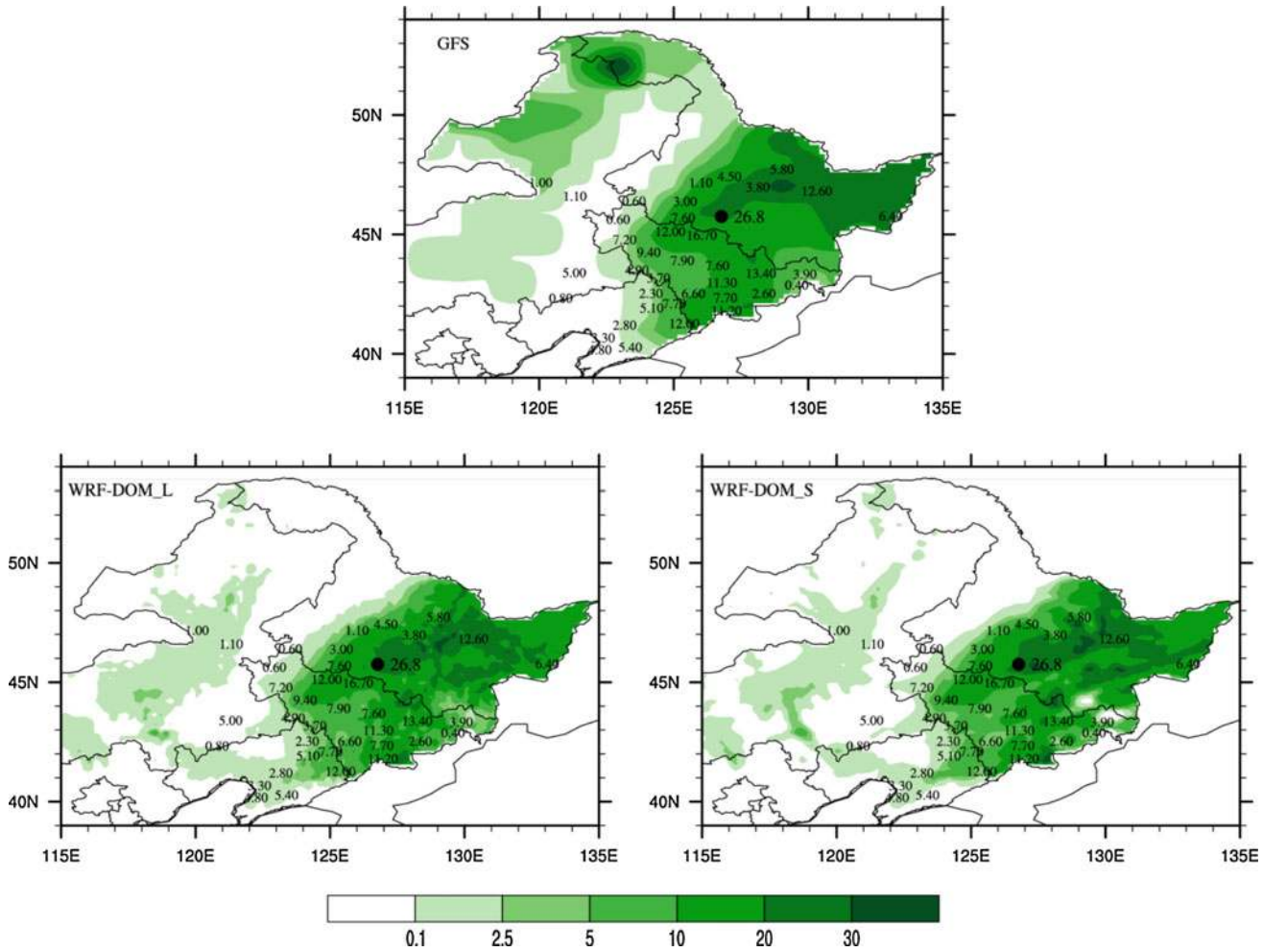

Fig. 12 Comparisons of simulated (*shading*) and observed (*marked with numbers*) 48-h accumulated water-equivalent snow (in mm) for GFS, DOM_L simulation and DOM_S simulations for 12–13 April

precipitation in South China is also reasonably reproduced in terms of magnitude, but the spatial location is still more southward in the simulation. The surface air temperature is also well reproduced by DOM_L for the NEC region and the whole of eastern China. The simulated surface air temperature is somewhat lower than the observed in northern NEC for 13 April.

We now discuss the DOM_S simulation on snowfall over NEC for 12–13 April. Figure 12 presents the DOM_S and DOM_L simulations in comparison with the GFS result and station observations over NEC. The GFS data set shows an inexistent area of snowfall over northern NEC. However, the WRF simulations did not make this mistake. In addition, the GFS overestimates the snowfall amount over the far eastern NEC. Both DOM_L and DOM_S well captured the snowfall in magnitude and spatial location over eastern NEC for the 2 days. The DOM_L and DOM_S simulation results are quite close to each other, because the two-way nesting approach was applied. However, there are still some quantitative differences between them, which will be shown in next section.

We further perform a quantitative analysis of the retrospectively forecasted water-equivalent snow for 48 h covering 12–13 April in comparison with the GFS and station observation data sets. Table 1 shows the results for 59 meteorological stations. Their averaged water-equivalent snow is 7.27 mm in the observation and 9.95 mm in the GFS. Therefore, the GFS overestimates the snowfall by about +37% (or +2.68 mm), with larger error in far eastern NEC. The DOM_L and DOM_S simulate 8.58 and 6.93 mm, respectively, with relative errors of +18% (or +1.31 mm) and −5% (or −0.34 mm). Therefore, the DOM_S simulation is much better than DOM_L, and both results are much closer to the observation as compared to the GFS in the station-based average.

The observed water-equivalent snow for Harbin, the capital of the Heilongjiang Province, is 26.8 mm. Results of GFS, DOM_L and DOM_S are 21, 28 and 27 mm,

Table 1 Observed and simulated 48-h accumulated water-equivalent snow (in mm) and other quantities for the stations during 12–13 April

Station number	Station name	Latitude	Longitude	Observed snow–water equivalent	WRF result of DOM_L	WRF result of DOM_S	GFS result	Error of DOM_L	Error of DOM_S	Error of GFS
50953	Harbin	45.75	126.77	26.8	28	27	21	1.2	0.2	−5.8
54063	Sanchahe	44.97	126	16.7	16	18	16	−0.7	1.3	−0.7
54094	Mudanjiang	44.57	129.6	16.6	24	2	15	7.4	−14.6	−1.6
54493	Kuandian	40.72	124.78	16.1	1	0	7	−15.1	−16.1	−9.1
54186	Dunhua	43.37	128.2	13.4	5	11	15	−8.4	−2.4	1.6
54377	Jian	41.1	126.15	13.3	19	3	11	5.7	−10.3	−2.3
50968	Shangzhi	45.22	127.97	13.2	20	4	15	6.8	−9.2	1.8
50853	Suihua	46.62	126.97	12.9	20	22	17	7.1	9.1	4.1
54363	Tonghua	41.68	125.9	12.9	9	6	12	−3.9	−6.9	−0.9
50873	Jiamusi	46.82	130.28	12.6	21	21	24	8.4	8.4	11.4
50949	Guoerluosi	45.12	124.83	12	16	15	15	4	3	3
54365	Hengren	41.27	125.35	12	4	4	7	−8	−8	−5
54273	Huadian	42.98	126.75	11.3	12	4	13	0.7	−7.3	1.7
54374	Linjiang	41.8	126.92	11.2	18	14	19	6.8	2.8	7.8
54181	Jiaohe	43.7	127.33	11.1	17	10	16	5.9	−1.1	4.9
54049	Changling	44.25	123.97	9.4	14	13	6	4.6	3.6	−3.4
50948	Qianan	45	124.02	9.2	9	8	9	−0.2	−1.2	−0.2
54284	Donggang	42.1	127.57	9.1	2	22	18	−7.1	12.9	8.9
54563	Wafangdian	39.63	122.02	8.5	0	0	0	−8.5	−8.5	−8.5
54134	Kailu	43.6	121.28	8.3	0	0	0	−8.3	−8.3	−8.3
54263	Panshi	42.95	126.05	8.2	8	6	8	−0.2	−2.2	−0.2
54346	Benxi	41.32	123.78	8.1	8	2	3	−0.1	−6.1	−5.1
54161	Changchun	43.9	125.22	7.9	6	8	9	−1.9	0.1	1.1
50877	Jingyu	46.3	129.58	7.8	17	21	18	9.2	13.2	10.2
54259	Qingyuan	42.1	124.92	7.7	7	6	9	−0.7	−1.7	1.3
54276	Jingyu	42.35	126.82	7.7	8	10	17	0.3	2.3	9.3
50950	Zhaozhou	45.7	125.25	7.6	16	12	11	8.4	4.4	3.4
54171	Yongji	43.7	126.52	7.6	14	8	13	6.4	0.4	5.4
54041	Tongyu	44.78	123.07	7.2	3	1	1	−4.2	−6.2	−6.2
54266	Meihekou	42.53	125.63	6.6	3	3	9	−3.6	−3.6	2.4
50983	Hulin	45.77	132.97	6.4	16	17	27	9.6	10.6	20.6
50888	Baoqing	46.32	132.18	6.3	19	16	26	12.7	9.7	19.7
50774	Yichun	47.73	128.92	5.8	9	7	19	3.2	1.2	13.2
54096	Suifenhe	44.38	131.15	5.7	8	20	6	2.3	14.3	0.3
54486	Xiuyan	40.28	123.28	5.4	0	0	0	−5.4	−5.4	−5.4
54351	Zhangdang	41.92	124.08	5.1	4	1	1	−1.1	−4.1	−4.1
54135	Tongliao	43.4	121.2	5	0	0	0	−5	−5	−5
54142	Shuangliao	43.5	123.53	4.9	3	3	5	−1.9	−1.9	0.1
54476	Xiongyue	40.17	122.15	4.8	0	0	0	−4.8	−4.8	−4.8
50756	Hailun	47.43	126.97	4.5	5	11	20	0.5	6.5	15.5
50788	Fujin	47.23	131.98	4	18	19	27	14	15	23
54339	Anshan	41.08	123	4	0	0	0	−4	−4	−4
54195	Wangqing	43.33	129.77	3.9	0	0	3	−3.9	−3.9	−0.9
50862	Tieli	46.98	128.02	3.8	13	5	24	9.2	1.2	20.2
54157	Siping	43.18	124.33	3.7	6	6	3	2.3	2.3	−0.7
54471	Yingkou	40.67	122.27	3.3	0	0	0	−3.3	−3.3	−3.3
50854	Anda	46.38	125.32	3	9	7	13	6	4	10
54342	Shenyang	41.2	123.07	2.8	0	0	0	−2.8	−2.8	−2.8

Table 1 continued

Station number	Station name	Latitude	Longitude	Observed snow–water equivalent	WRF result of DOM_L	WRF result of DOM_S	GFS result	Error of DOM_L	Error of DOM_S	Error of GFS
54285	Songjiang	42.53	128.25	2.6	11	3	15	8.4	0.4	12.4
54254	Kaiyuan	42.53	124.05	2.3	3	1	4	0.7	−1.3	1.7
54333	Xinmin	41.98	122.83	1.7	0	0	0	-1.7	−1.7	−1.7
54386	Changbai	42.35	128.17	1.3	23	1	16	21.7	−0.3	14.7
50758	Mingshui	47.17	125.9	1.1	7	7	13	5.9	5.9	11.9
50834	Suolun	46.6	121.22	1.1	0	0	1	−1.1	−1.1	−0.1
50727	Aershan	47.17	119.95	1	0	0	3	−1	−1	2
54226	Baoguotu	42.33	120.7	0.8	0	0	0	−0.8	−0.8	−0.8
50844	Tailai	46.4	123.42	0.6	0	0	1	−0.6	−0.6	0.4
50936	Baicheng	45.63	122.83	0.6	0	0	0	−0.6	−0.6	−0.6
54292	Yanji	42.88	129.47	0.4	7	4	6	6.6	3.6	5.6
				7.27	**8.58**	**6.93**	**9.95**	**1.31**	**−0.34**	**2.68**

The numbers in bold indicate the multi-station averaged result

indicating that the DOM_S simulation is the best among them.

5 Summary and discussion

During 12–13 April 2010, an exceptionally strong snowfall occurred in Northeast China, with 26.8 mm of accumulated water-equivalent snow over Harbin. The snowstorm occurred in an unusually late part of the year, especially when a warming trend was observed in NEC for the past few decades, and it brought record-breaking snowfalls over the NEC regions. About 10 days before the snowstorm, the Siberia High intensified and shifted southeastward. It cut off the low-pressure system over NEC and strengthened the East Asian Trough. Large convergence of water vapor and strong rising motion clearly occurred over eastern Northeast China, resulting in heavy snowfall.

Experiments with the WRF model in this work show a general success for forecasting the HS1004. The two-way nesting simulations can capture many features of the heavy snowstorm including snowfall amount and the large-scale and regional circulation anomalies associated with the snowstorm. The WRF hindcast experiment overcame the inexistent snowfall over the northern NEC and simulated spatial distribution and magnitude of the snowfall amount with a higher degree of accuracy for the 59 stations' mean result. The NEC nested domain simulation DOM_S is even better than the simulation within the mother domain DOM_L.

Given the reasonable skill of the WRF model in simulating the HS1004 event, this study provides an encouraging result for applying the WRF model in forecast of NEC snowfalls. The forecast result from the nested forecast system is very promising for an operational purpose. Undoubtedly, experiments with more heavy snowfall cases should be performed to obtain more robust conclusions and to better understand the systematic errors of models for the region. As a matter of fact, most of the heavy snowstorm cases in the NEC region in the past 40 years have just been tested by this approach, and the results are similarly encouraging and will be submitted for publication.

Acknowledgments This research was supported by the Major State Basic Research Development Program of China (973 Program) under Grant No. 2009CB421406, the Chinese Academy of Sciences under Grant KZCX2-YW-Q1-02, Special Fund for Public Welfare Industry (Meteorology) (GYHY200906018) and the National Natural Science Foundation of China under Grant 40821092. Our thanks are due to Prof. Lijuan Chen of the National Climate Center, China Meteorological Administration, for her assistance in using the station data set for Northeast China.

References

Changnon SA, Changnon D, Karl TR (2006) Temporal and spatial characteristics of snowstorms in the contiguous United States. J Appl Meteor Climatol 45:1141–1155. doi:10.1175/JAM2395.1

Dudhia J (1989) Numerical study of convection observed during the winter monsoon experiment using a mesoscale two-dimensional model. J Atmos Sci 46:3077–3107

Gambo K, Lu L, Li WJ (1987) Numerical simulation of Eurasian teleconnection pattern in atmospheric circulation during the Northern Hemisphere winter. Adv Atmos Sci 4:385–394. doi:10.1007/BF02656739

Gong DY, Wang SW, Zhu JH (2001) East Asian winter monsoon and Arctic Oscillation. Geophys Res Lett 18:2073–2076

Hong S, Noh Y, Dudhia J (2006) A new vertical diffusion package with an explicit treatment of entrainment processes. Mon Wea Rev 134:2318–2341

Jeong J-H, Kim B-M, Ho C-H, Chen D, Lim G-H (2006) Stratospheric origin of cold surge occurrence in East Asia. Geophys Res Lett 33:L14710. doi:10.1029/2006GL026607

Kain JS, Fritsch JM (1993) Convective parameterization for mesoscale models: the Kain-Fritsch scheme, the representation of cumulus convection in numerical models. Meteor Monogr 46:165–170

Kocin PJ, Uccellini LW (2004) A snowfall impact scale derived from northeast storm snowfall distributions. Bull Amer Meteor Soc 85:177–194

Liu YQ, Giorgi F, Washington WM (1994) Simulation of summer monsoon climate over East Asia with a NCAR regional climate model. Mon Wea Rev 122:2331–2348

Liu YQ, Avissar R, Giorgi F (1996) A simulation with the regional climate model RegCM2 of extremely anomalous precipitation during the 1991 East Asian flood: an evaluation study. J Geophys Res 101:26199–26215

Liu YQ, Fan GZ, Zhou DW (2008) Numerical simulation of summer precipitation in China by using a regional climate model (RegCM3). J Chengdu Univ Info Tech 23:442–447 (in Chinese)

Liu YL, Yu HM, Ren GY, Zhou JX (2010) Temporal and spatial variation characteristics of the snow storms in Heilongjiang Province during 1961–2006. Climatic Envir Res 15:470–478 (in Chinese)

Mlawer E, Taubman S, Brown P, Iacono M, Clough S (1997) Radiative transfer for inhomogeneous atmospheres: RRTM, a validated correlated-k model for the longwave. J Geophys Res 102:16663–16682

Purser RJ, Fujita T, Sar SK, Michalakes JG (2001) A semi-Lagrangian dynamical core for the non-hydrostatic WRF model. Preprints, Ninth Conference on Mesoscale Processes, Ft. Lauderdale, FL, Amer Meteor Soc, CD-ROM, J5.3

Qin HF, Jin RH (2008) Numerical simulation study of the cause of snowstorm process in Northeast China on 3–5 March 2007. Meteorol Mon 34:30–38 (in Chinese)

Simmons A, Uppala S, Dee D, Kobayashi S (2007) ERA-Interim: new ECMWF reanalysis products from 1989 onwards. Newsletter 110—Winter 2006/07, ECMWF, 11 pp

Sun JQ, Wang HJ, Yuan W (2009) A preliminary investigation on causes of the catastrophic snowstorm in March, 2007 in northeastern part of China. Acta Meteorologica Sinica 67:469–477 (in Chinese)

Sun JQ, Wang HJ, Yuan W, Chen HP (2010) Spatial–temporal features of intense snowfall events in China and their possible change. J Geophys Res 115:D16110. doi:10.1029/2009JD013541

Thompson DWJ, Wallace JM (1998) The Arctic Oscillation signature in the wintertime geopotential height and temperature fields. Geophys Res Lett 25:1297–1300

Wallace JM, Gutzler DS (1981) Teleconnections in the geopotential height field during the Northern Hemisphere winter. Mon Wea Rev 109:784–812

Wang JZ, Ding YH (1995) Research of moist symmetric instability in a strong snowfall in North China. Acta Meteorologica Sinica 53:451–460 (in Chinese)

Wang HJ, Jiang DB (2004) A new East Asian winter monsoon intensity index and atmospheric circulation comparison between strong and weak composite. Quat Sci 24:19–27 (in Chinese with English abstract)

Xu GK, Zhao SX, Wang YG (2007) Experiment of ensemble forecast of heavy rainfall in the Huaihe River during rainy season of 2003. Climatic Envir Res 12:481–488 (in Chinese)

Xue F, Wang HJ, He JH (2003) Interannual variability of Mascarene high and Australian high and their influences on summer rainfall over East Asia. Chin Sci Bull 48(5):492–497

Zhang F, Snyder C, Rotunno C (2002) Mesoscale predictability of the "surprise" snowstorm of 24–25 January 2000. Mon Wea Rev 130:1617–1632

Zielinski GA (2002) A classification scheme for winter storms in the eastern and central United States with an emphasis on nor'easters. Bull Amer Meteor Soc 83:37–51